JOURNAL OF MATERIALS SCIENCE **38** (2003) 2727–2742

Influence of the additives and processing conditions on the characteristics of dense SnO_2-based ceramics

D. NISIRO, G. FABBRI, G. C. CELOTTI, A. BELLOSI
ISTEC-CNR, Institute of Science and Technology for Ceramics, Faenza, Italy
E-mail: bellosi@istec.cnr.it

Three different SnO_2-based powder mixtures, containing 2 wt% CuO as sintering aid and Sb_2O_3 in amounts from 0 to 4 wt% as activator of the electrical conductivity, were sintered to high density at temperatures in the range 1000–1400°C and soaking times from 1 to 6 h. Densification behaviour and microstructure development are strongly dependent on the presence of CuO, that gives rise to a liquid phase, and on Sb_2O_3 that retards the liquid phase formation and hinders grain growth. Cu and Sb cations can enter s.s. in the SnO_2 network with different oxidation states and in different positions, depending on the sintering conditions. The characteristics of the grain boundary phase, of the SnO_2 solid solutions and their modification depending on thermal treatments were analyzed. The electrical resistivity values varied in a wide range from 10^{-1} to 10^4 Ωcm, depending on starting composition and processing conditions: in terms of the final density and of the electrical conductivity, the optimal sintering conditions were found to be 1200°C, for 1–3 h. The electrical resistivity was related to the microstructural features, particularly to the characteristics of the resulting SnO_2-based solid solutions.

1. Introduction

In recent decades tin-dioxide-based ceramics have been studied and developed for numerous fields of application such as electronics, electrotechniques, electrochemistry, catalysis, biotechnology, nuclear technology, chemical technologies, metallurgy. In fact SnO_2 is a semiconductor (*n*-type) with wide band gap (3.6 eV) which exhibits interesting properties depending on the microstructural features of the material. On one hand, highly porous tin oxide polycrystals presenting structural defects are suitable for use as a catalyst (e.g., in organic synthesis) and as semiconductor gas sensors [1–4]. For example, oxygen vacancies formed in sensitive surface layers of porous SnO_2-based ceramics act as sites of physisorption or chemisorption of atmospheric oxygen, which is of key importance in gas sensing. On the other hand, dense SnO_2 ceramics, owing to their semiconducting properties, find some structural applications such as electrodes for high temperature uses, namely for aluminium electrolysis and the glass industry [5, 6]. Recently, additional potential applications of tin dioxide have been considered, such as electrochromic devices, crystal displays, photodectectors and various electrical devices (e.g., igniters, heaters). The wide spectrum of applications demands strict control of the properties, a control that is possible to the extent that the specific correlations between composition, structure and physico-chemical and mechanical properties required by each case are established.

Unfortunately, additive-free SnO_2 exhibits poor sinterability, probably due to the dominance of non-densifying mechanisms for mass transport, such as surface diffusion and evaporation/condensation [7–10] which only promote pore coarsening and grain growth. Also the densification of pure SnO_2 can be strongly limited by the vaporization of tin monoxide which should occur at a high rate, above 1100°C.

Several routes can be followed to improve sinterability of SnO_2: the use of very fine powders compacted under high pressure [11, 12], the densification using hot isostatic pressing [13, 14], the addition of a series of oxides (individuals and various combinations), namely ZnO [9, 15, 16], MnO [8, 15–18], CoO [8, 17], Fe_2O_3 [15], TiO_2 [15], V_2O_5 [19], Nb_2O_5 [9, 20, 22], Sb_2O_3 [16], Li_2O [22] and CuO [7, 10, 16, 23–27]. CuO is particularly effective, because it improves densification also at low concentrations (1 mol%) [28] through the formation of a liquid phase. The eutectic of the Cu–O system is at 1080°C, while a liquid phase exists in the Sn–Cu–O_2 system at 940°C [25]. In the system SnO_2–CuO between 940 and 1000°C densification is controlled by the dissolution process and, at higher temperature, the transfer of material is limited by liquid-state diffusion [28]. For sintering temperature lower than 940°C several mechanisms have been proposed to explain the improvement of densification of copper oxide-doped tin oxide. Some authors assumed that solid state bulk diffusion is activated by the formation of lattice defects due to the dissolution of Cu(II)

in the SnO_2 network [25], whereas others attributed the densification to a fast copper distribution on the SnO_2 grain surface. On the other hand, copper oxide additions were proved [29] to stabilize ultrafine microstructure of SnO_2, due to the decrease of the grain boundary mobility under specific processing conditions.

In order to develop electroconductive bulk dense ceramics based on SnO_2 an additional kind of activator, besides the sintering aid, is required e.g., additives that promote electrical conductivity, such as Nb_2O_5, V_2O_5, Sb_2O_3 [15, 16, 30–34].

A large discrepancy exists between the results of the electrical behaviour obtained for single crystals, porous and dense polycrystalline ceramics, especially for pure and weakly doped materials; several microstructural and structural factors influence the electrical behaviour. Results obtained for highly dense ceramics showed that the existence of the grain boundary potential barrier in SnO_2-based materials can be an intrinsic property of solid/solid interfaces [32].

The electrical properties of dense SnO_2-based ceramics sintered with the aid of CuO are strongly sensitive to the type and amount of a second additive present. It was reported that at room temperature the conductivity of SnO_2 varies from 1 to 2×10^{-12} $(\Omega\ cm)^{-1}$ depending on the nature of the additive. The features affecting the electrical behaviour are strongly dependent on the dopant, for example the electrical conductivity of Ta- and Nb-doped ceramics are controlled by grain boundary effects at low temperature [32], while the addition of Sb_2O_3 causes a segregation of antimony and copper at the grain surface and the disappearance of the grain boundary effects [32].

In addition, antimony oxide was proved to be the most effective as it also increases the electrical conductivity of SnO_2 owing to the increased charge carrier concentration. The amount of added Sb_2O_3 generally ranges from 1 to 4 wt%. The introduction of Sb^{5+} within the rutile type network of tin oxide acts as an electron donor and improves the electrical conductivity dramatically (by 4–5 orders of magnitude). The law of mass action for non-stoichiometric tin dioxide showed that an increase of electron concentration is compensated by a decrease of oxygen vacancies.

On the other hand, antimony oxide reduces the sinterability of tin oxide, both in the case of pure SnO_2 and of SnO_2 doped with sintering aids, therefore several combinations of additives promoting at the same time sintering and electrical conductivities were tested [9, 15, 32, 34]. The best results were obtained with a combined addition of Sb_2O_3 and CuO [7, 15, 27, 30, 32, 35, 37]. Although several possible combinations of these additives has been tested, the concurrent influence of both the additives on the densification, microstructure and electrical conductivity of SnO_2-based ceramics has not been systematically investigated and conflicting results are shown about the relationships between composition-microstructure and properties. The effects of the processing conditions on microstructural modifications have been often disregarded, in fact studies on the electrical conductivity of SnO_2-based ceramics reveal the major influence exerted by the nature of the doping agent and the thermal treatment conditions (temperature, time, atmosphere), but incontestable relationships among composition, processing and electrical conductivity were not assessed.

The effects of different amounts of Sb_2O_3 (up to 10%) were studied regarding the microstructural and structural modifications and the reactions among the constituent phases [7, 30, 36–43]. The information on the interaction of SnO_2 with Sb_2O_3 and CuO, which might be of primary importance for establishing the optimum composition of the starting powder mixtures, are scarce and contradictory. It is generally accepted that the solubility of Sb_2O_3 in SnO_2 is limited (up to 20–30 at% Sb can be dissolved in the lattice of SnO_2) [30, 37]. However the solid solution is metastable and phase separation to Sb_2O_4 and SnO_2 occurs at high temperature [37]. The phenomenologies occurring in the ternary system SnO_2–Sb_2O_3–CuO [15, 30, 33, 36] are strongly influenced not only by the starting compositions but also by the environmental conditions, in particular the oxygen partial pressure during the heat treatments.

Some authors obtained highly dense electroconductive ceramics in the system SnO_2–Sb_2O_3–CuO through sintering in the temperature range 1400–1500°C [7, 16].

The aim of this study is to produce structural fully dense SnO_2-based ceramics and to define the processing conditions that make it possible to obtain materials having different and controlled electrical conductivities. SnO_2-based ceramics with CuO and Sb_2O_3 added were sintered at different temperatures (in the range 1000–1400°C) and times (from 1 to 6 h) in order to study the microstructure modification and to identify the factors influencing the electrical properties.

2. Experimental procedure

The types and characteristics of the starting raw materials are shown in Table I.

The following powder mixtures (amounts in wt% and in mol%) were prepared by ball milling in water for 12 h adding 2 wt% of polyethylene glycol (PEG), drying at 80°C for 24 h and sieving.

A: $98SnO_2 + 2CuO$	(wt%)
$96SnO_2 + 4CuO$	(mol%)
B: $96SnO_2 + 2CuO + 2Sb_2O_3$	(wt%)
$95SnO_2 + 4CuO + 1Sb_2O_3$	(mol%)
C: $94SnO_2 + 2CuO + 4Sb_2O_3$	(wt%)
$94SnO_2 + 4CuO + 2Sb_2O_3$	(mol%)

TABLE I Starting powders characteristics: s.s.a.: specific surface area BET, m.g.s.: mean particle size, p.s.r: particle size range

	s.s.a. ($m^2\ g^{-1}$)	m.g.s. (μm)	p.s.r. (μm)	Chemical purity (wt%)
SnO_2 (Aldrich)	8.37	0.10	0.02–5	99.9
CuO (Merck)	6.72	0.14	0.1–0.2	99.0
Sb_2O_3 (Aldrich)	2.56	0.45	0.5–2	99.0

Green samples having the shape of a bar were produced by uniaxial pressing at 200 MPa. The green densities were about 58% for the different mixtures.

The samples were sintered in air at the following temperatures 1000, 1200, 1300, 1350, 1400°C for different soaking times (1, 3, 6 h). The densities of the sintered samples were measured by the Archimedes method.

The microstructure of the sintered materials were analyzed by scanning electron microscopy (SEM) on fracture, polished and etched surfaces. Thermal etching treatments were performed on polished surfaces at temperature 50–100°C lower than the sintering temperature, for 15 min.

The concentration of the additives and the composition of grain boundary phases were determined by electron probe microanalysis (EDX). Crystalline phases were detected by XRD on polished surfaces of the sintered samples.

Selected samples were powdered for the measurement of the lattice parameter of the SnO_2 s.s. with the X-ray diffractometer, using Ni-filtered CuKα radiation, with scanning speed of 0.8°/min within the range 125–150° (2θ). The cell parameters were refined using 5 reflections (*521*, *440*, *323*, *530*, *512*). Silicon powder was used as an internal standard. The accuracy of the lattice parameters a and c of the tetragonal cell were within 0.00005 nm for a and 0.00003 nm for c.

For the measurement of the electrical conductivity, the upper surface and the two edge surfaces were polished in order to remove possible thin surface scale induced by diffusion or evaporation during sintering. The electrical resistivity was measured using the four probe DC method at room temperature, inducing a longitudinal current along the bar specimens of $2 \times 2.5 \times 25\ mm^3$. The current and the voltage were detected at the same time in two different digital high-resolution multimeters. In order to neglect the increase of temperature of test bars during the measurements due to Joule effects, the selected constant current for each sample was that corresponding to the same total power dissipation (under 0.1 W in each cases). The resistivity values were determined from the electrical resistance measurements taking into account of the test leads distance and cross section area of the samples.

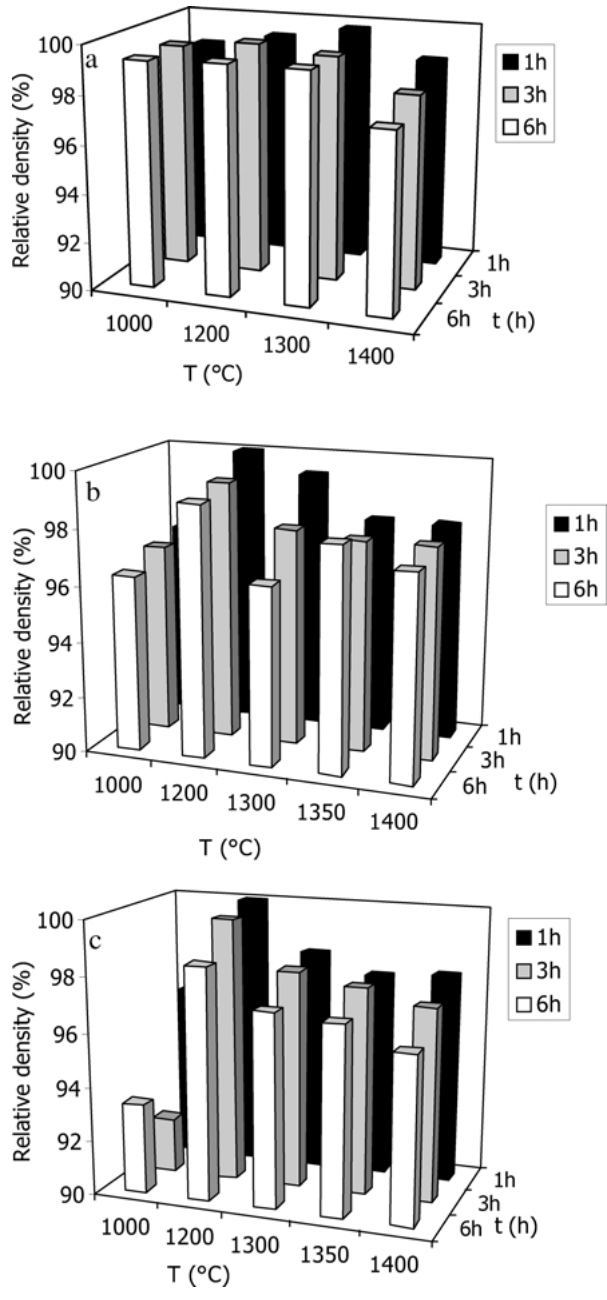

Figure 1 Relative densities, in function of the sintering temperature and time, of the samples of composition: (a) A (SnO_2 + 2 wt%CuO), (b) B (SnO_2 + 2 wt%CuO + 2 wt%Sb_2O_3), and (c) C (SnO_2 + 2 wt%CuO + 4 wt%Sb_2O_3).

3. Results

3.1. Sintering behaviour

The density of the sintered ceramics is strongly sensitive to the composition, the sintering temperature and the holding time in temperature.

Composition A (SnO_2 + 2CuO) (Fig. 1a) reaches nearly full densities (from 99.1 to 99.8%) in the temperature range 1200–1300°C, although a slight density decrease is observed as the soaking time increases. At 1000°C the relative density is about 99%, while at very high temperature (1400°C) a linear decrease from 99% to 97% is observed as the soaking time increases from 1 to 6 h.

Composition B, containing 2% Sb_2O_3, reached full density (Fig. 1b) at 1200°C 1 h, about 98% at 1300°C, about 97% at 1350 and 1400°C. In all cases the long exposure to temperature (6 h) favoured a decrease in density of 1–2%. The lowest density was measured after sintering at 1000°C.

Composition C, containing 4% of Sb_2O_3, showed high relative densities (about 99%, Fig. 1c) after sintering at 1200°C for all soaking times and at 1300°C for 1 h. Lower densities (about 96%) were measured on samples treated at 1000°C, at 1300°C for 3–6 h, at 1350 and 1400°C for every exposure time.

The general trends revealed in Fig. 1a–c are the following: (i) the optimal sintering conditions for the production of high density SnO_2-based ceramics are: temperature 1200°C and soaking time 1–3 h. Under these processing conditions, all the compositions tested reach 99–100% of relative density and (ii) at lower (1000°C) and higher (1300–1400°C) temperatures the density decreases with increasing soaking time and with the

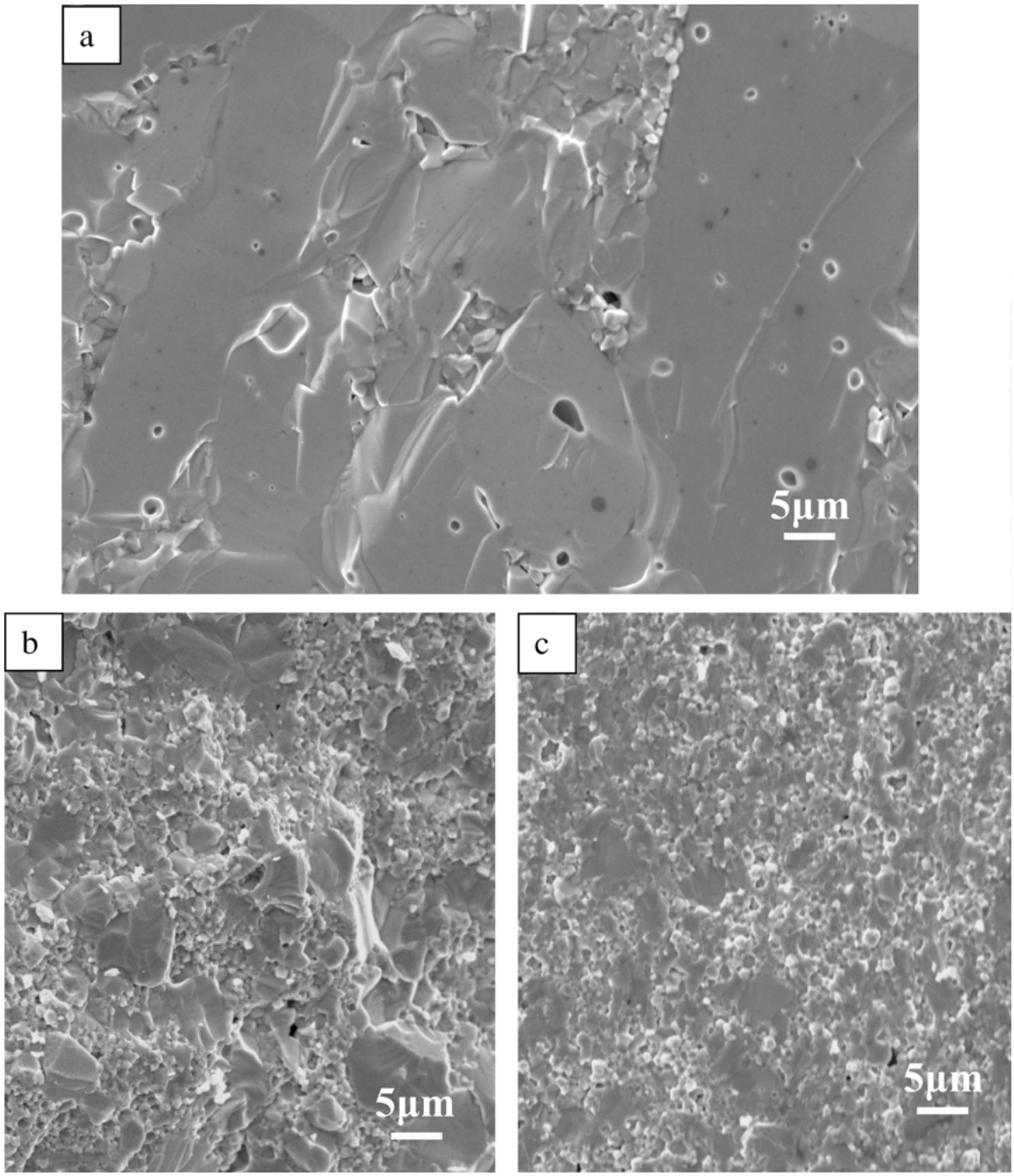

Figure 2 Fracture surfaces of the samples sintered at 1200°C for 1 h, relatively to the compositions: (a) composition A (SnO_2 + 2 wt%CuO), (b) composition B (SnO_2 + 2 wt%CuO + 2 wt%Sb_2O_3), and (c) composition C (SnO_2 + 2 wt%CuO + 4wt%Sb_2O_3).

amount of Sb_2O_3, in fact the samples from composition A, without Sb_2O_3, have the highest densities among the tested ones.

3.2. Evolution of the microstructure

3.2.1. Crystalline phases

The only significant crystalline phase revealed by X-ray diffraction on the polished surfaces of all the sintered materials is SnO_2 solid solutions with rutile-type structure: it suggests a partial substitution of antimony and/or of copper in the SnO_2 crystals. The presence of traces of crystalline Sb_2O_4 and $CuSb_2O_6$ cannot be excluded. On the other hand, a concentration of CuO and $Cu_4SbO_{4.5}$ was detected on the surface of the as sintered samples.

3.2.2. Morphology and grain size

Figs 2a–c, 3a–d and 4a, b show the variation of the morphology of the SnO_2-based ceramics depending either on the starting composition or on the different processing conditions. Materials from composition A, containing SnO_2 + 2 wt% CuO, undergo a fast grain growth during sintering; the high grain boundary mobility entraps pores within the grains also at relatively low temperature. An example relative to the material sintered at 1200°C is shown in Fig. 2a, where grains well exceeding 50 μm coexist with very small grains of few microns. Generally the fracture is transgranular in correspondence to the large grains and intergranular in correspondence to the small ones. Secondary phase precipitated at grain boundaries was observed in samples sintered at 1200 and

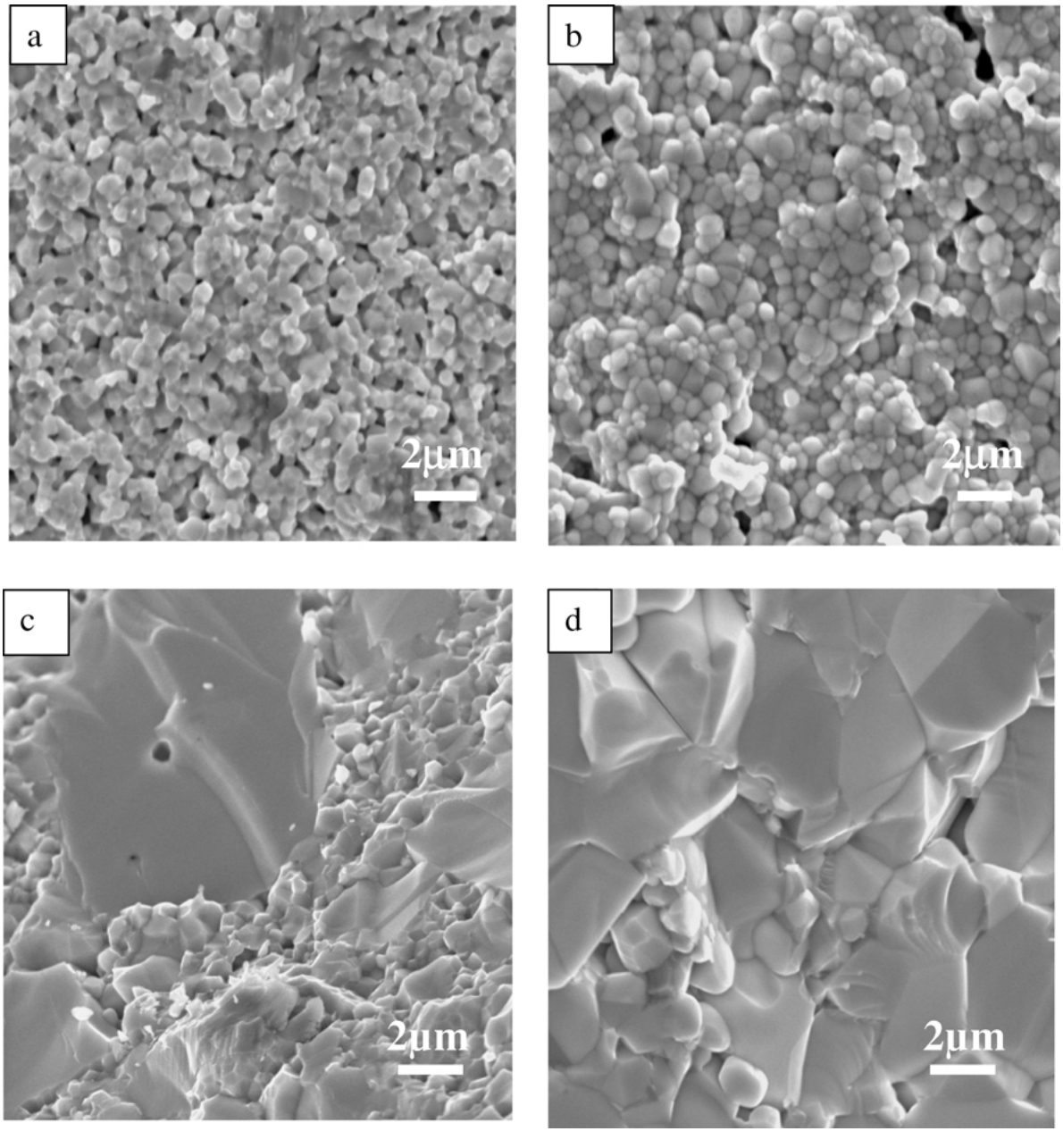

Figure 3 Fracture surfaces of the samples of composition B(SnO_2 + 2 wt%CuO + 2 wt%Sb_2O_3), sintered at: (a) 1000°C, 1 h, (b) 1000°C, 6 h, (c) 1200°C, 1 h, and (d) 1200°C, 6 h.

1300°C, for all the compositions, while no grain boundary phases were detected after sintering at 1350 and 1400°C.

Figs 2, 3 and 4 highlight the effect of Sb_2O_3 on the microstructure of these Sn-based ceramics. At all the sintering temperatures, increasing the amount of Sb_2O_3 leads to microstructures with decreasing grain size and improved homogeneity of the grain morphology: an example is shown in Fig. 2a–c, that compares the microstructure of materials A, B and C sintered at 1200°C for 1 h. The sintering temperature has a strong effect on grain size distribution and grain shape, while the soaking time in temperature is less effective on the microstructure evolution. Independently of composition, the materials sintered at 1000°C have globe-shaped grain with uniform size. Mean grain size is about 0.5 μm for sample A and about 1 μm for the two Sb_2O_3-doped materials B and C; an example is shown in Fig. 3a–b for material B. From these micrographs it is evident that in samples sintered at 1000°C for 1 h there is some degree of intergranular porosity, while in samples sintered for longer soaking time porosity is nearly absent, and, although very limited, grain growth did occur.

Sintering temperatures in the range 1200–1300°C induce a relevant change in the morphology (examples are shown in Figs 3c–d and in Fig. 5). A bimodal grain size and shape is always observed, which makes it impossible to estimate a mean grain size. Some of the grains undergo a fast grain growth: abnormal grains have irregular shape and dimensions in the range 10–50 μm, while the smallest grains are equiaxial with dimensions 2–5 μm. The percentage of large grains increases with the increase of the sintering parameters: time and temperature. Materials sintered at temperatures higher than 1300°C have a more uniform microstructure, although very coarse (Figs 4a and b). Grain size ranges from 10 to 30 μm; intergranular

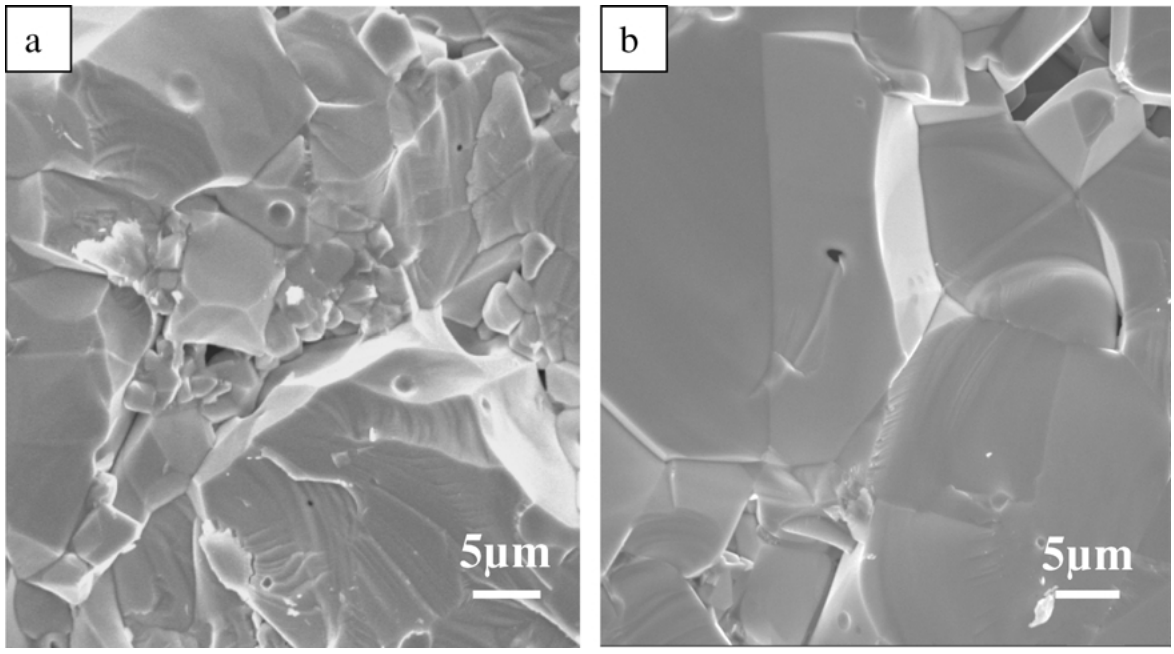

Figure 4 Fracture surfaces of the samples of composition B(SnO_2 + 2 wt%CuO + 2 wt%Sb_2O_3), sintered at: (a) 1300°C, 3 h and (b) 1400°C, 3 h.

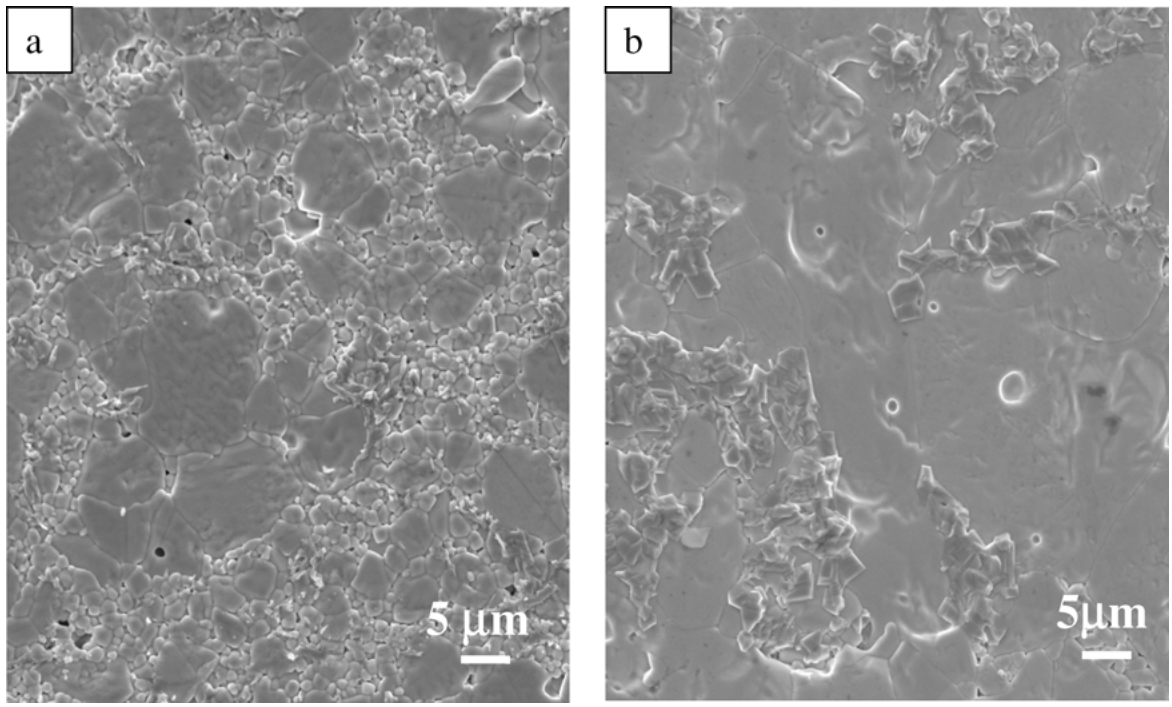

Figure 5 Microstructures of the polished and etched surfaces of the samples: (a) composition B (SnO_2 + 2 wt%CuO + 2 wt%Sb_2O_3), sintered at 1200°C, 1 h and (b) composition C (SnO_2 + 2 wt%CuO + 4 wt%Sb_2O_3), sintered at 1200°C, 6 h.

pores, some microcracks and absence of grain boundary phases are revealed.

3.2.3. Phase composition and grain boundary phases

As previously mentioned, in the CuO-containing ceramics (composition A) part of the small SnO_2 grains are surrounded by (or embedded in) an intergranular phase (see an example in Fig. 6) while the larger grains have rather clean boundaries. As grain size increases, the grain boundary phase shrinks and then disappears almost completely at temperatures higher than 1300°C.

EDX analyses carried out on polished surfaces (Figs 7 and 8) show that this phase is copper rich, which means that it corresponds to copper-oxide residues. SEM and EDX observations also confirm that there is solubility of Cu in SnO_2, in agreement with previous results [10, 25]: in fact Cu was found not only in the grain boundary pockets, but also in the small SnO_2 grains. Although with the available technique it is not possible to investigate the evolution of the copper concentration as a function of the distance from the surface of a grain, the presence of copper was ascertained at the boundaries of the largest grains, however the presence of Cu in the centres of these grains was not detected.

On compositions B and C, glassy pockets containing small (1–2 μm) grains are sometimes found among large grains: in Fig. 9a and b examples are shown

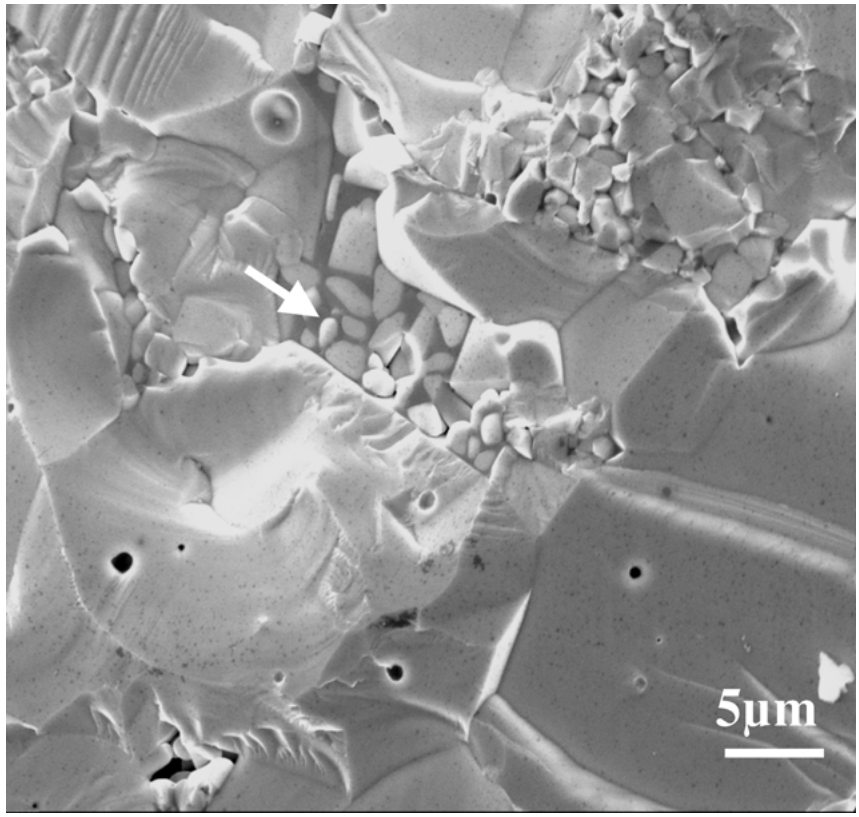

Figure 6 Fracture surfaces of the samples of composition A (SnO_2 + 2 wt%CuO), sintered at 1200°C for 1 h, showing the presence of grain boundary phase in correspondence of the areas where small grains concentrate.

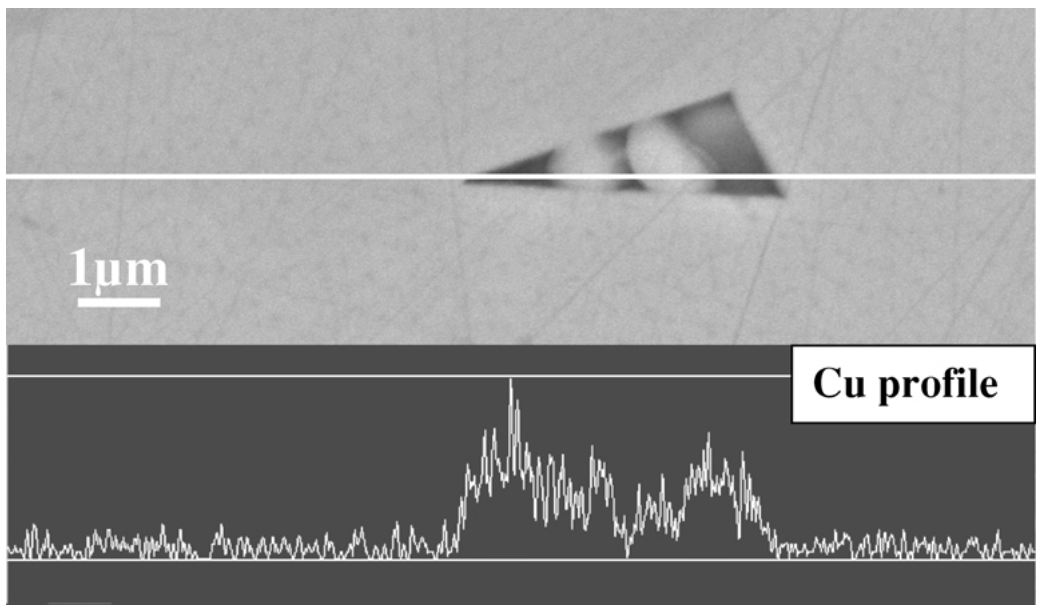

Figure 7 Grain boundary phase revealed on the polished surface of composition A (SnO_2 + 2 wt%CuO), sintered at 1200°C for 1 h: morphology and concentration profile of copper.

relative to a polished surface of material B sintered at 1200°C for 1 h and to the fracture surface (Fig. 9c) of material B sintered at 1300°C for 3 h. The EDX analyses reveal that this secondary phase contains, besides Sn, both Cu, in large amount, and Sb in low amounts.

3.2.4. Effects of the thermal etching

The thermally etched surfaces highlight the grain boundaries and the location of the intergranular phases. As evident from Fig. 10a and b (for materials from composition A) and Fig. 11a–d (for materials from compositions B and C), new small crystals either isolated or piled up are found in patches, particularly evident at triple points or in the correspondence of small SnO_2 grains. These crystals form during the etching thermal treatments at 1150°C (this temperature being higher than the temperature at which liquid phase forms), either from the melting of the grain boundary phase or from phase separation (e.g., diffusion of the additives at the solid/solid interface) and subsequent melting. During cooling these phases crystallise and the newly

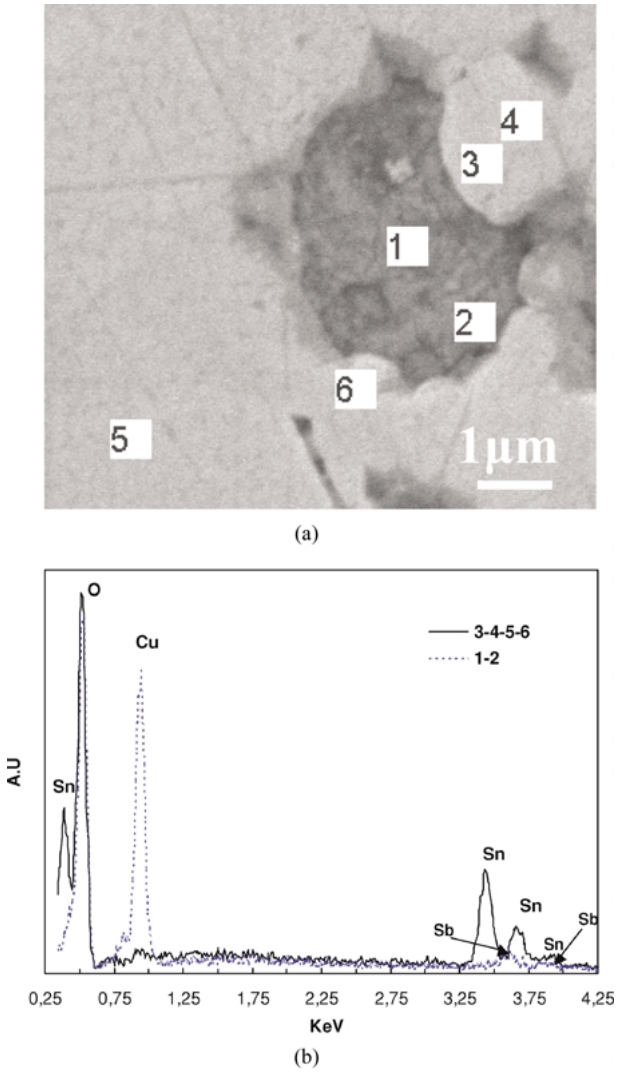

Figure 8 Grain boundary phase revealed on the polished surface of composition B (SnO_2 + 2 wt%CuO + 2 wt%Sb_2O_3) sintered at 1200°C for 1 h: (a) morphology, and (b) EDX spectra showing the concentration of Cu in the grain boundary phase, that also contains low amounts of Sb.

formed crystals come out of the grain boundaries or triple points and appear in relief in respect with the original polished surface. Figs 10 and 11 point out the following features concerning the formation of the crystalline phases during the thermal etching:

- in samples sintered at 1000°C and at 1200°C for 1 h (Fig. 11b), very few isolated crystals formed, emerging from the SnO_2 s.s. grains.
- as the sintering temperature or time is raised, increasing amounts of clumps of crystals are concentrated in correspondence to the areas where the small grains are located; on the contrary the main part of the boundaries between the largest grains appear completely free from secondary phases (Figs 11c and d).
- X-ray diffractograms indicated that in materials from composition A (SnO_2 + CuO), these crystals consist of copper rich phases (CuO), while in materials B and C the crystalline phases are CuO and $Cu_4SbO_{4.5}$.

The morphological aspects observed on the etched surfaces confirm also that Sb_2O_3 acts as grain growth inhibitor, in direct relationship to its amount, as is evident from a comparison of the microstructures of materials B and C, both sintered at 1200°C for 1 h. Picture 11c shows also that some grains are surrounded by a thick layer of Cu- and Sb-rich phase, in samples sintered for short times, up to 3 h at 1200°C. As a consequence of longer exposure to high temperature (e.g., 6 h at 1200°C and at higher temperatures, Fig. 11d), this intergranular layer disappears and the amount of crystals, which accumulates on the surface during the thermal etching, increases.

3.2.5. Solid solutions and lattice parameters

The EDX analyses revealed the presence of Cu and Sb inside the SnO_2 grains, but the concentration of these elements could not be assessed. The observed inhomogeneities in the distribution of Cu and Sb are related to the grain size, presence of grain boundary phases, phase separations and segregation phenomena. Therefore, to investigate the relative and mutual solubilities of the involved phases and their evolution as a function of the processing conditions, more accurate analyses were performed by the measurement of lattice parameters on selected samples. The results, shown in Table II, indicate a variation of the lattice parameters depending on both composition of the materials and sintering parameters. The lattice parameters determined for pure SnO_2 are in good agreement with the ASTM-file: we found $a = 0.47385$ nm and $c = 0.31869$ nm for the starting powders, very close to the data in the JCPDS card N° 41–1445, that indicates $a = 0.47382$ and $c = 0.31871$ nm.

Material A. The small but significant variations in lattice parameters revealed in materials from composition A show that CuO is involved in formation and subsequent modifications of the SnO_2 solid solutions, in any case its presence induces a lattice contraction. The following results were found (Fig. 12a and b):

- the smallest dimension of the SnO_2 s.s. lattice is measured in materials sintered at 1000°C. As the sintering temperature increases ($T = 1200$ and 1300°C, 1 h), about the same cell dimensions (i.e. cell volume)

TABLE II Lattice parameters of the SnO_2 s.s

Sample	a (nm) ± 0.00005	c (nm) ± 0.00003
A, 1000°C, 1 h	0.47357	0.31860
A, 1200°C, 1 h	0.47377	0.31861
A, 1300°C, 1 h	0.47370	0.31860
A, 1400°C, 1 h	0.47368	0.31868
A, 1200°C, 6 h	0.47368	0.31876
B, 1000°C, 1 h	0.47351	0.31864
B, 1200°C, 1 h	0.47369	0.31848
B, 1300°C, 1 h	0.47368	0.31873
B, 1400°C, 1 h	0.47379	0.31883
C, 1000°C, 1 h	0.47327	0.31820
C, 1200°C, 1 h	0.47350	0.31839
C, 1300°C, 1 h	0.47376	0.31877
C, 1400°C, 1 h	0.47382	0.31895
C, 1400°C, 6 h	0.47385	0.31885

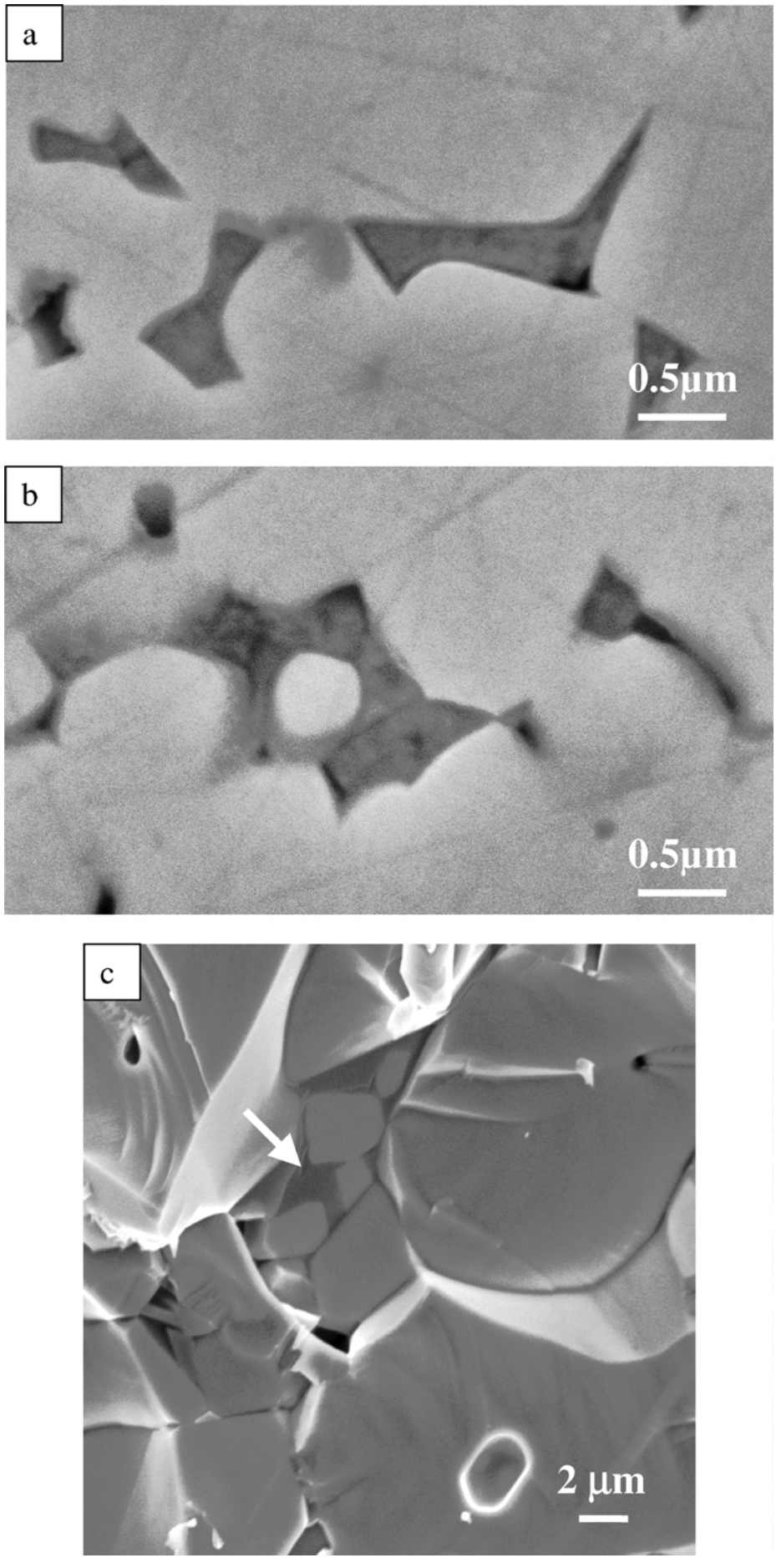

Figure 9 Grain boundary phase observed in the sample of composition B (SnO_2 + 2 wt%CuO + 2 wt%Sb_2O_3): (a and b) sintered at 1200°C, 1 h (polished surface), and (c) sintered at 1300°C, 3 h (fracture surface).

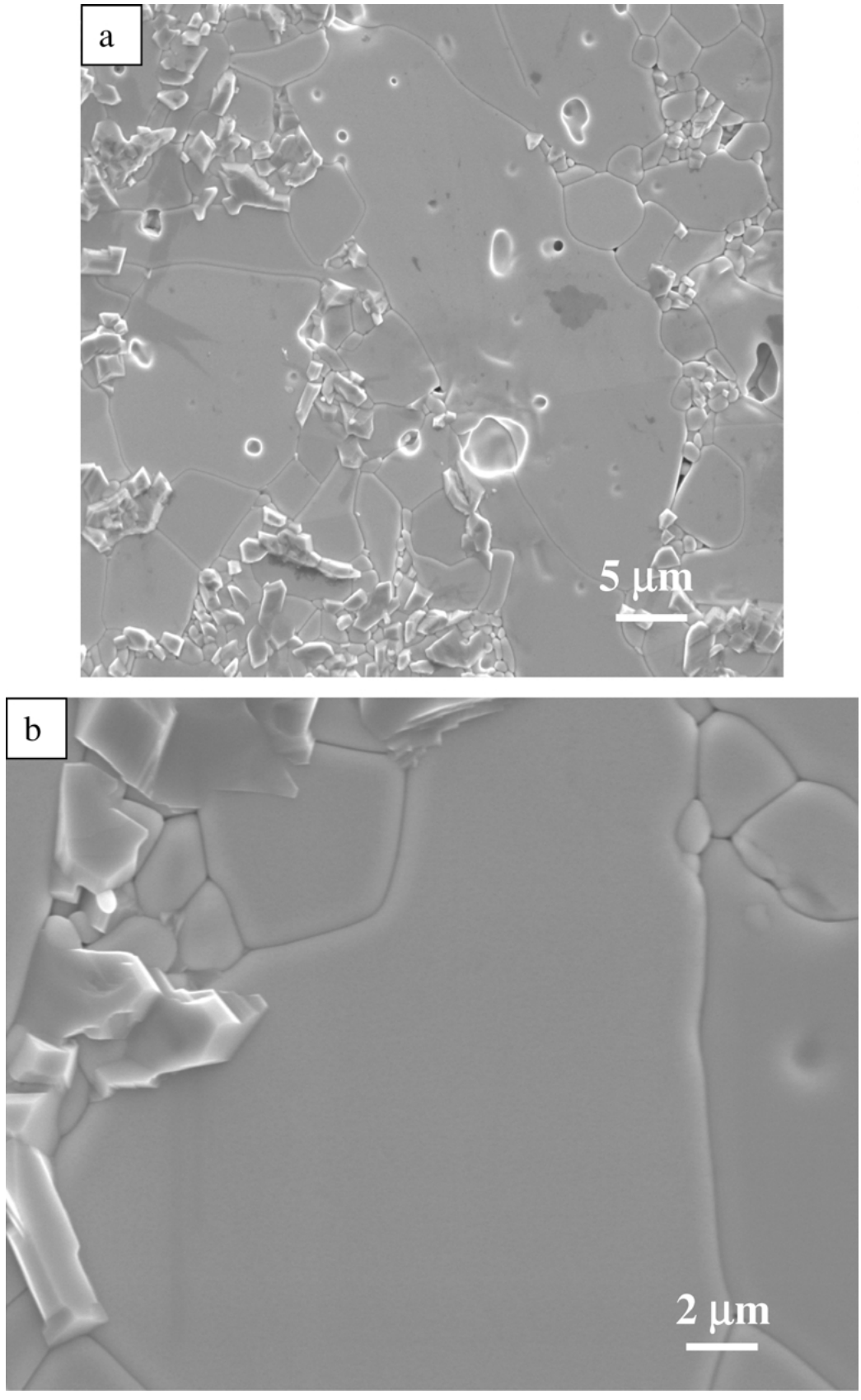

Figure 10 Morphology of the thermally etched surfaces of materials of composition A (SnO_2 + 2 wt%CuO), sintered at: (a) 1200°C, 1 h and (b) 1200°C, 6 h.

were found, still lower than the undoped SnO_2, but slightly higher than the values measured in the material sintered at 1000°C.

– when the sintering time is very long (see the data relative to 1200°C for 6 h) the *c* axis of the rutile network becomes still larger and the cell volume, although even lower than that of undoped SnO_2, is enhanced as well.

Materials B and C. The formation of the solid solution is favoured by the comparable ionic radii of Sn^{4+} (0.067 nm) and Sb^{5+} (0.062 nm) ions [44], which means

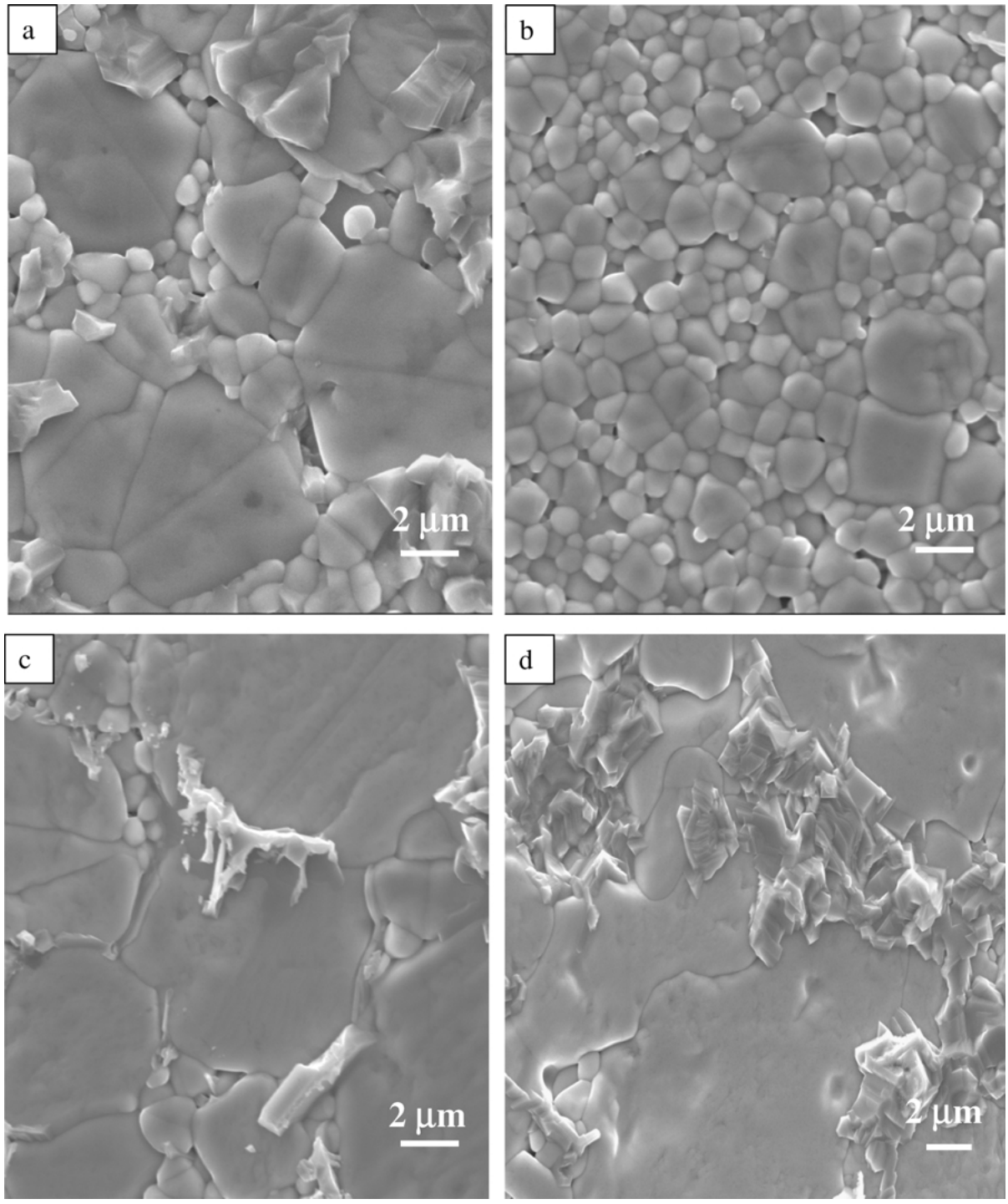

Figure 11 Morphology of the thermally etched surfaces of the following samples: (a) composition B (SnO_2 + 2 wt%CuO + 2 wt%Sb_2O_3) sintered at 1200°C, 1 h, (b) composition C (SnO_2 + 2 wt%CuO + 4 wt%Sb_2O_3) sintered at 1200°C, 1 h, (c) composition B (SnO_2 + 2 wt%CuO + 2 wt%Sb_2O_3) sintered at 1200°C, 6 h, and (d) composition C (SnO_2 + 2 wt%CuO + 4 wt%Sb_2O_3) sintered at 1200°C, 6 h.

that a small solubility of Sb_2O_3 in SnO_2 is not expected to change the cell parameters of the solid solution very much.

The contraction of the rutile-type network of the SnO_2 s.s., compared to undoped SnO_2, detected in materials sintered at 1000°C and 1200°C is followed by an increase of both the parameters in materials sintered at higher temperature. While the *a* axis becomes equal to that of undoped tin oxide in materials from composition C sintered at 1400°C, *c* axis increases up to levels higher than that of undoped SnO_2 in materials sintered at 1300 and 1400°C (Fig. 12). The cell volumes calculated from the measured parameters indicate that the volume expansion of the SnO_2 s.s. lattice overcomes that of undoped SnO_2 after sintering at temperatures higher than about 1400°C.

3.3. Electrical resistivity

Materials from composition A reveal the following ranges of resistivity (Fig. 13): (i) higher than 10^3 Ωcm in materials sintered at 1000°C, (ii) ranging from 10 to 50 Ωcm in samples sintered at 1200°C, (iii) ranging from 1 to 10 Ωcm in samples sintered at 1300–1400°C for 1 and 3 h, (iv) sintering for long time (6 h) induces an increase of the resistivity from 10 to 100 Ωcm.

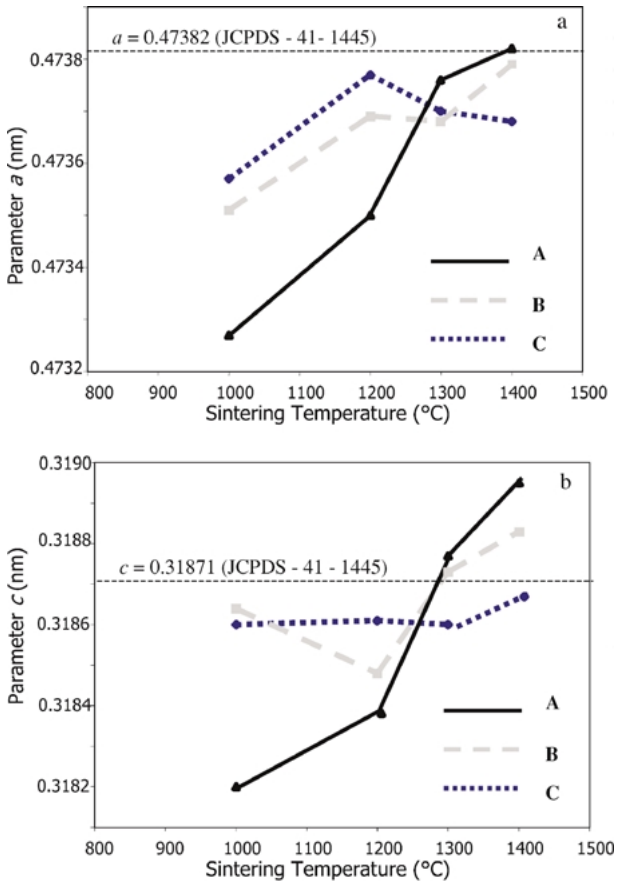

Figure 12 Variation of the cell parameters measured on samples of the three tested compositions, in function of the sintering temperature (the time of exposure is constant, 1 h): (a) parameter *a* and (b) parameter *c*.

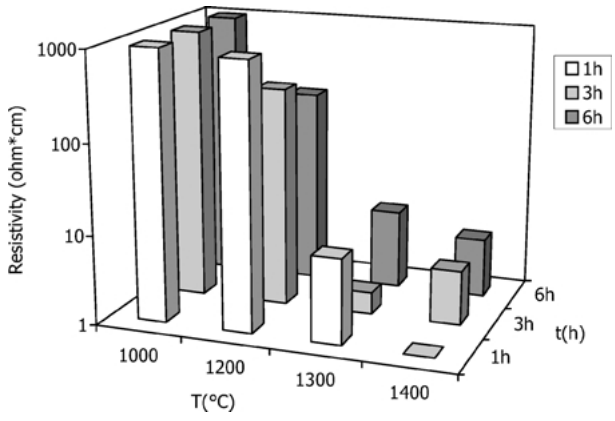

Figure 13 Electrical resistivity of the materials of the composition A (SnO_2 + 2 wt%CuO), in function of the sintering parameters: temperature and time.

Fig. 14a and b show the electrical resistivity for ceramics produced from the systems B and C. There is a wide spread of results, particularly regarding the samples sintered at 1000°C and at 1350–1400°C. Rather regular trends are identified for materials sintered at 1200°C and at 1300°C.

Materials doped with 2 wt%Sb_2O_3 + 2 wt%CuO have very low resistivity if sintered at 1200°C for 1 and 3 h, but there is a sharp increase in the values of resistivity in materials sintered at 1300°C.

In all the cases, there is a trend towards the increase of the resistivity with the increase of the sintering time.

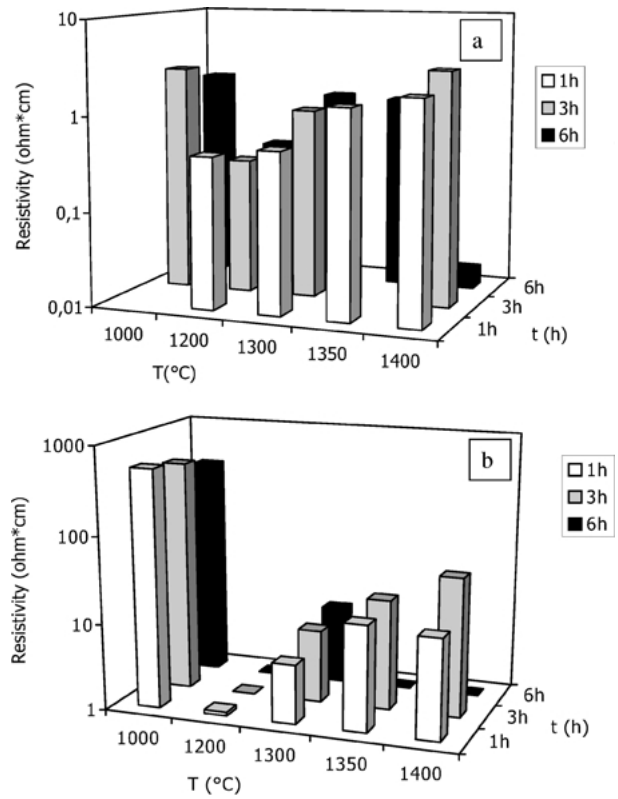

Figure 14 Electrical resistivity of the materials of the composition B (SnO_2 + 2 wt%CuO + 2 wt%Sb_2O_3) and C (SnO_2 + 2 wt%CuO + 4 wt%Sb_2O_3) in function of the sintering parameters: temperature and time.

4. Discussion

4.1. Densification and microstructure

As previously reported in many studies [7, 23–25], the densification of SnO_2 is strongly enhanced by addition of a small amount of copper. In the present study, already at 1000°C a high densification level was achieved, enabled by the low temperature melt in the system Sn–Cu–O_2, that occurs at 940°C [24–26]. The enhanced densification and grain growth at temperatures higher than about 1200°C indicates the presence of an additional amount of liquidus, that formed at 1090°C [10] from the eutectic CuO–CuO_2. The accumulation of Cu (and of low amounts of Sb) in the grain boundary phase was detected in the samples sintered at temperature lower than about 1200°C and for short soaking times.

The relative low densities observed in materials sintered at temperatures higher than 1300°C and for long times can be due to the progressive consumption of the liquid phase, because the Cu and Sb cations enter in solid solution in the SnO_2 cell. As a consequence of the reduction and disappearance of the liquid phase, solid state diffusion mechanisms favour a fast grain boundary mobility, resulting in grain coarsening and in an amount of intragranular porosity, in agreement with previous studies [24, 39].

Generally the effects of antimony oxide on the densification behaviour were not investigated, however Las et al. [32] suggested that a $CuSb_2O_6$-like compound could be formed, reducing the formation of the liquid phase in the system CuO–Cu_2O. The observed

evolution of the microstructure in relationships with the composition (Fig. 2) confirms that antimony oxide retards grain growth to an extent directly dependent on its amount and lowers the final density, at constant sintering conditions, compared to materials containing only CuO as additive. Moreover, the highest densities are obtained when the Sb_2O_3 content is as large as the copper content: the excess of dopant hinders the sinterability, in agreement with previous results [7, 40].

The above reported remarks confirm that, during sintering, the relative contribution of material transport mechanisms and of the interaction among the involved species depend on the processing conditions and powder characteristics. The control of microstructure is difficult, as, usually, densification and grain growth occur simultaneously.

In all the samples, the observed microstructural evolution highlights the fact that the solubility of copper inside the SnO_2 grains is sufficient to consume progressively the whole liquid. Factors difficult to control are the surface segregation of the additives during sintering (CuO and $Cu_4SbO_{4.5}$ were clearly detected on the surface of the sintered samples) and phenomena involving vaporization of tin monoxide and of Sb oxides, confirmed by the weight loss and by the microstructure of the external surface of the samples. In addition, the antimony content within the SnO_2 solid solutions decreases gradually owing to antimony diffusion towards the particle surface, followed by vaporization.

The mass transfer of part of the additives towards the sample surface, where they segregate, and partly evaporate, leads to the depletion of grain boundaries and triple points, consequently the final density is relatively lower after sintering at very high temperatures and for long soaking times.

4.2. Cell parameters

The only phase constituting the sintered bulk materials is SnO_2 s.s; the substitution of antimony and/or copper for tin is revealed by the variation of the lattice parameters of SnO_2. Previous studies show different contradictory results about the solid solutions that can be formed in the SnO_2–CuO–Sb_2O_3 system [10, 24, 30, 32, 33, 35, 37, 38, 41]. Sb and/or Cu ions can enter solid solutions either in substitution or interstitial positions. Contradictory assessments are reported in literature about the role of copper: Santilli *et al.* [23] claim that copper ions do not enter into the crystal structure of SnO_2, while Lalande *et al.* [10] and Dolet *et al.* [25] assert the evidence of Cu diffusion into SnO_2.

In our samples A no residual CuO is present in all the sintered materials; the cell dimensions and the calculated corresponding cell volumes in materials from composition A sintered at 1000°C sustain the hypothesis that nearly all the added CuO (2 wt%) entered s.s. in substitutional position of Sn^{4+} (0.069 nm), the copper cation being Cu^{3+} (0.054 nm).

The modification of the SnO_2 s.s. in material A, at increased sintering temperature and time, can be due to one or more of the following features:

(i) part of the Cu changes its valence, resulting in a larger ion, but remains in substitution of Sn^{4+},

(ii) part of Cu^{3+} ion inserts interstitially into the tin oxide network,

(iii) part of CuO must be eliminated by diffusion towards the sample surface where it segregates.

To understand which one of these phenomena is prevailing, these data are discussed later in relation to the electrical conductivity values.

The decrease of the cell dimensions revealed in the ceramics from compositions B and C sintered at 1000 and 1200°C confirms the solubility of both antimony and copper oxide in the rutile network. The calculated values of the cell volume in samples B sintered at 1000 and 1200°C are in agreement with the hypothesis that all the Cu^{3+} and Sb^{5+} (0.060 nm) cations of the dopants are introduced in the Sn^{4+} position. A particular case is that of material C sintered at 1000°C. The excess of Sb-dopant could have induced a reticular disorder, as broadened peaks were clearly revealed on the x-ray diffractograms. This evidence, combined with the very low lattice parameters (both *a* and *c*) could be due to an altered co-ordination number of Sn (that is normally 6): at least 10% of Sn ions could have a co-ordination number of 5, as predicted by our calculations.

To explain the modification of the SnO_2 rutile cell as a function of the sintering parameters (temperatures >1200°C) for materials belonging to compositions B and C, again the change of the valence could provide an answer. In fact, the presence of the smallest dopant cations as Cu^{3+} and Sb^{5+} results in the lowest cell dimension, as accepted for materials sintered at 1000°C.

If the cation valence changes to different combinations (Cu^{2+} (0.073 nm) and or Sb^{3+} (0.076 nm)) the lattice size increases. The heterovalent mixture $Sb^{3+}Sb^{5+}O_2$ must be the component of the solid solution in the sample sintered in the temperature range 1200–1400°C, since the ionic radius of Sb^{3+} is large enough to expand the SnO_2 lattice, compared to the ionic radius of Sn^{4+} (0.069 nm). If a fixed amount of Sb^{3+} ion is present, the same amount of chemically bonded Sb^{5+} can be present as well in the solid solution.

The same effect of the cell dilatation also appears as a consequence of: (i) the insertion of copper or antimony interstitially in the tin-oxide network. This latter case seems particularly true in the material sintered at 1400°C, because the relative diffractograms reveal modifications of peak intensities that could be ascribed to interstitial position of the dopant cations; (ii) the reduction of the ion amounts, e.g., by partial evaporation or surface segregation of the dopant oxides, mainly of Sb^{3+} ions [45, 46].

4.3. Relationships between electrical conductivity and microstructure

Basically SnO_2-based ceramics are *n*-type semiconductors with donor levels (about 0.03 eV) very close to the bottom of the conduction band [47, 48]: the electrical conductivity is improved by the addition of Sb_2O_3, due to a higher donor level concentration near the conduction band in the grains and/or to a lower electron trap

concentration at the grain boundary (e.g., lower interfacial charge) [32].

The plots in Figs 13 and 14 show the variability of the electrical resistivity as a function of the composition and of the sintering conditions, and confirm that the microstructure and density play an important role in the electrical properties. Bulk SnO_2-based ceramics are apparently single phase: this means that the dopant solubility and/or phase precipitation at grain boundaries control electrical properties.

Material A. The effect of Cu on SnO_2 grain conductivity has not been defined. Previous results appear conflicting: Las *et al*. [32] suggest a strong increase of the resistivity due to the addition of copper oxide; values of resistivity higher than 10^{11} Ωcm were measured at room temperature on materials sintered at 1150°C. Dolet *et al*. [24] showed that copper dissolves into the SnO_2 rutile-type structure and that the electrical behaviour of the material is in agreement with the interstitial position for Cu^{2+} ions. An additional hypothesis points out that the incorporation of Cu^{2+} ions into SnO_2, assessed by IR data [44], should determine the increases of the ionic character of the lattice.

In the present case, some relationships between the cell parameters and the electrical behaviour are suggested:

(i) in material sintered at 1000°C, the introduction of Cu^{3+} ions in Sn^{4+} position slightly increases the free electron concentration and, therefore, the *n*-type conductivity in comparison with pure SnO_2.

(ii) both the values of the electrical resistivity and of the cell parameters of materials sintered at 1200–1400°C are indicative of the insertion of part of Cu^{3+} ions interstitially into the tin dioxide network. Consequently, the free electron concentration increases and hence the *n*-type conductivity also.

The other possible explanation, suggested above to explain the slight increase of the lattice volume (e.g., the change in the valence of Cu ions—in substitution of Sn^{4+}—from the smallest one Cu^{3+} to the larger ions Cu^{2+} or Cu^{1+}), is not supported by the strong decrease of the electrical resistivity of these ceramics.

However, the variation of the electrical resistivity within the range 0.5–20 Ωcm depends also on other microstructural parameters such as grain size, type and characteristics of the grain boundaries.

Materials B and C. On the basis of the results about the Cu-doped SnO_2, it is evident that the difference in the electrical behaviour observed in materials containing CuO and Sb_2O_3 depends on a combination of effects coming from both the dopants, and, particularly, on the oxidation state and on the position of Sb cations. In fact, when in interstitial position, whatever the oxidation state, there is an increase in the electron concentration (e.g, a decrease of the electrical resistivity) associated to a lattice dilatation.

If Sb is in a substitutional position, depending on the oxidation state, different situations can occur:

(i) Sb^{5+}: the lattice may contract owing to the low ionic size; the rise in electron concentration increases the electrical conductivity.

(ii) Sb^{4+}: such a cation can increase the electrical conductivity of SnO_2 grains only if it contributes to the formation of donor levels very close to the conduction band [32]. However Sb^{4+} is more likely substituted by antimony cations with mixed valence Sb^{5+} and Sb^{3+}.

(iii) Sb^{3+}: the substitution of Sn^{4+} by Sb^{3+} in the rutile-type structure of SnO_2 leads to a decrease in the predominant *n*-type electrical conductivity.

In addition to the above described features, other microstructural factors influence the electrical behaviour. Grain size and grain boundary characteristics are important, but mainly the attention must be given to the extent of the true solid solution, that may vary with the sintering temperature and time. The solid solution is metastable and, consequently patches of segregated antimony and copper oxides may occur on the surface. The latter processes were considered in the explanation of the apparent *p*-type behaviour of reduced conductivity in materials containing relatively high quantities of Sb_2O_3 [41].

Another important factor is the possible inhomogeneous additive distribution inside SnO_2 grains. Cu and Sb were found more concentrated in the smaller grains than inside the large ones, that generally appear additive free. Besides, chemical gradients were observed near grain boundaries in the large grains, although it was not possible to investigate the concentration profiles.

Being so complex the phenomena that affect the electrical behaviour of SnO_2 doped with CuO and Sb_2O_3, it is impossible to define the role of each structural or microstructural parameter.

However, the definition of the position of Cu and Sb cations in the SnO_2 lattice on the basis of the cell parameters and of the electrical measurement can be attempted. The cell size allows us to hypothesise that in materials sintered below 1300°C solid solutions contain Cu^{3+} and Sb^{5+} ions in substitutional position. The low electrical resistivity in materials sintered at 1200°C confirms this hypothesis. On the contrary, to explain the high electrical resistivity in materials sintered at 1000°C (that are characterized by the lowest lattice size) other determining factors have to be considered, such as some residual porosity, presence of grain boundary phases, incomplete additive distribution inside the grains.

The lattice contraction, compared to the size of the undoped SnO_2 (but the cell size is slightly higher than in the material sintered at 1000°C), measured in materials sintered at 1300 and 1400°C (particularly the increase of the *c*-axis of the s.s.), can be caused by a combination of Cu and Sb cations with mixed valences Sb^{5+} and Sb^{3+} (e.g., the presence of ions with larger radius in substitutional position) or by the presence of the same ions in interstitial position. This latter case seems to explain the very low electrical resistivity of the sample C sintered at 1400°C for 6 h.

The analyses of the obtained data, relative to materials sintered at 1200–1300°C (Fig. 14) indicate that raising the concentration of Sb_2O_3 and CuO above 2 mass% apparently is ineffective with respect to the densification and, consequently, to the electrical conductivity of SnO_2-based ceramics.

5. Conclusions

Fully dense electroconductive SnO_2-based ceramics were produced using 2 wt%CuO as sintering aid and 2 wt% Sb_2O_3 to activate electronductivity. Higher amounts of Sb_2O_3 lowers sinterability and improves electrical resistivity. The sintering behaviour and the microstructural evolution are dependent on the liquid phase characteristics and on concurrent phenomena occurring at the same time, such as:—mass tranfer that induces sintering,—phase segregation at grain boundaries,—phase evaporation (Sb oxides and tin monoxide) at the sample surface,—formation of solid solutions, where Sb and Cu cations enter in substitutional or interstitial position with different valence, depending on the sintering temperature and time. The optimum sintering parameters are: temperature 1200°C and time in the range 1–3 h. Lower and higher temperatures do not allow near fully dense materials. In particular, at temperatures higher than 1300°C enhanced grain growth occurs, accompanied by partial diffusion towards the sample surface of antimonium oxide and its subsequent vaporization. The electrical resistivity values varied in a wide range from 10^{-1} to 10^4 Ωcm, depending on starting composition and processing conditions; they are related to the microstructural features, particularly to the characteristics (oxidation state and position of the dopant cations) in the resulting SnO_2-based solid solutions. The lowest resistivity values were measured on sample of the composition SnO_2 + 2 wt%CuO + 2 wt%Sb_2O_3, sintered at 1200, for 1–3 h: under these conditions the electrical conductivity is due to Sb^{5+} ions located in substitutional position within the SnO_2 cell.

It was found that in particular conditions also CuO-doped tin oxide can became electroconductive, in fact materials from composition SnO_2 + 2 wt%CuO revealed a resistivity in the range 0.5–20 Ωcm, when sintered at 1300–1400°C, due to the insertion of Cu^{3+} ions interstitially in the SnO_2 network.

References

1. D. PYKE, R. REID and R. J. TILLEY, *J. Chem. Soc. Faraday Trans. I* **76** (1980) 1174.
2. T. SEIYAMA, N. YAMAZAE and H. ARAI, *Sensors and Actuators* **4** (1983) 85.
3. K. IHOKURA, K. TANAKA and N. MURAKAMI, *ibid.* **4** (1983) 607.
4. M.FORSTER, J. EBERLE, S. STRAISSLER and G. PFISTER, *Inst. Phys. Ser.* **111** (1990) 479.
5. W. ZIEMBA and B. ZIEMBA, *Szklo i Ceram.* **24** (1973) 12.
6. T. CHAVATAL, *Sprechsaal Keram. Glass Baust B* **107** (1974) 1057.
7. P. H. DUVIGNEAUD and D. REIGHARD, in "Sience of Sintering. Vol 12, edited by P. Vincenzini (Ceramurgia srl. Faenza. Italy, 1980) p. 287.
8. J. A. CERRI, E. R. LEITE, D. GOUVEA and E. LONGO, *J. Am. Ceram. Soc.* **79**(3) (1996) 799.
9. K. KIMURA, S. INADA and T. YAMAGUCHI, *J. Mater. Sci.* **24** (1989) 220.
10. J. LALANDE, R. OLLITRAULT-FICHET and P. BOCH, *J. Europ. Ceram. Soc.* **20** (2000) 2415.
11. E. R. LEITE, J. A. CERRI, E. LONGO, J. A. VARELA and C. A. PASKOCIMA, *ibid.* **21** (2001) 669.
12. J.-P. AHN, J.-K. PARK and M.-J. HUH, *J. Am. Ceram: Soc.* **80** (1997) 2165.
13. M. YOSHINAKA, K. HIROTA, M. ITO, H. TAKANO and O. YAMAGUCHI, *ibid.* **82** (1999) 220.
14. *Idem., ibid.* **82** (1999) 216.
15. S. ZUCA, M. TERZI, M. ZAHARESCU and K. MATIASOVSKI, *J. Mat. Sci.* **26** (1991) 1673.
16. T. MATSUSHITA and I. YAMAI, *Yogyo Kyokai Shi* **80** (1972) 305.
17. J. A. VARELA, J. A. CERRI, E. R. LEITE, E. LONGO, M. SHAMSUZZOHA and R. C. BRADT, *Ceram.Int.* **25** (1999) 253.
18. D. GOUVEA, A. SMITH, J. P. BONNET and J. A. VARELA, *J. Europ. Ceram. Soc.* **18** (1998) 345.
19. J. TAKAHASHI, K. KODAIRA, T. MATSUSHITA, I. YAMAI and H. SAITO, *Yogyo Kyokai Shi.* **83** (1975) 33.
20. J. TAKAHASHI, I. YAMAI and H. SAITO, *ibid.* **83** (1975) 362.
21. G. E. S. BRITO, S. H. PULCINELLI, C. V. SANTILLI and N. BARELLI, *J. Mat. Sci Lett.* **12** (1993) 992.
22. D. W. YUAN, S. F. WANG, W. HUEBNER and G. SIMKOVICH, *J. Mater. Res.* **8** (1993) 1675.
23. C. V. SANTILLI, S. H. PULCINELLI, G. E. S. BRITO and V. BRIOIS, *J. Phys. Chem. B* **103** (1999) 2660.
24. N. DOLET, J. M. HEINTZ, M. ONILLON and J. P. BONNET, *J. Europ. Ceram. Soc.* **9** (1992) 19.
25. N. DOLET, J. M. HEINTZ, L. RABARDEL, M. ONILLON and J. P. BONNET, *J. Mat. Sci.* **30** (1995) 365.
26. J. P. BONNET, N. DOLET and J. M. HEINTZ, *J. Europ. Ceram. Soc.* **16** (1996) 1163.
27. S. MIHAIU, O. SCARLAT, GH. ALDICA and M. ZAHARESCU, *ibid.* **21** (2001) 1801.
28. J. A. VARELA, O. J. WITTEMORE and E. LONGO, *Ceram Int.* **16** (1990) 177.
29. C. XU, J. TAMAKI, N. MIURA and N. YAMAZOE, *J. Mater. Sci.* **27** (1992) 963.
30. M. ZAHARESCU, S. MIHAIU, S. ZUCA and K. MATIASOVSKY, *ibid.* **26** (1991) 1666.
31. D. R. ORÒLIK, M. I. IAVANOVSKAYA and A. CH. GURLO, *J. Anal. Chem.* **52** (1997) 59.
32. W. C. LAS, N. DOLET, P. DORDOR and J. P. BONNET, *J. Appl. Phys.* **74**(10) (1993) 6191.
33. M. R. SAHAR and M. HASBULLAH, in "Third Euro-Ceramics Vol. 2," edited by P. Duran, J. F. Fernandez (Faenza Editrice Iberica, Spain, 1993) p. 455.
34. M. S. CASTRO and C. M. ALDAO, *J. Europ. Ceram. Soc.* **18** (1998) 2233.
35. S. ZUCA, G. ALDICA, M. S. MIHAIU and M. ZAHARESCU, in "9th Cimtec-World Ceramic Congress. Ceramics: Getting into the 2000's—Part. A," edited by P. Vincenzini (Techna srl, Faenza, Italy, 1999) p. 354.
36. M. ZAHARESCU, S. MIHAIU, D. CRISAN and S. ZUCA, in "Third Euro-Ceramics," Vol. 2," edited by P. Duran and J. F. Fernandez (Faenza Editrice Iberica, Spain, 1993) p. 359.
37. T. KIKUCHI and M. UMEHARA, *J. Mat. Sci Lett.* **4** (1985) 1051.
38. D. E. DYSHEL, *Inorganic Mat.* **32** (1996) 51.
39. J. A. VARELA, O. J. WHITTMORE and M. J. BALL, in "Sintering'85," edited by G. C. Kuczynski, D. P. Uskokovich, H. Palmour III and M. M. Ristic (Plenum Press, New York, 1987) p. 259.
40. J. GALASIU, R. GALASIU, N. POPA and V. CHIVU, *Rev. Roumaine de Chim.* **42** (1997) 349.
41. A. OVENSTON, D. SPRINCEANA, J. R. WALLS and M. CALDARARU, *J. Mater. Sci.* **29** (1994) 4946.
42. O. JONESCU, R. MARCHIDAN, S. MIHAIU, M. ZAHARESCU and D. CRISAN, *Key Engineering Mater.* **132–136** (1997) 848.

43. M. STAN, S. MIHAIU, D. CRISAN and M. ZAHARESCU, *ibid.* p. 790.
44. R. D. SHANNON, *Acta Crystall.* **A32** (1976) 751.
45. G. B. HOFLUND, D. F. COX, G. L. WOODSON and H. A. LAITINEN, *Thin Solid Films* **78** (1981) 357.
46. P. A. COX, R. G. EGDELL and C. HARDING, *Surf. Svi.* **123** (1982) 179.
47. C. G. FONSTAD and R. REDIKER, *J. Appl. Phys.* **42** (1971) 2911.
48. S. SAMSON and C. G. FONSTAD, *ibid.* **44** (1973) 4618.

Received 2 April 2002
and accepted 27 February 2003